Nonlinear effects in the bounded dust-vortex flow in plasma

Modhuchandra Laishram,* Devendra Sharma, Prabal K. Chattopdhyay, and Predhiman K. Kaw
Institute for Plasma Research, HBNI, Bhat, Gandhinagar 382428, India
(Received 26 September 2016; revised manuscript received 17 January 2017; published 13 March 2017)

The vortex structures in a cloud of electrically suspended dust in a streaming plasma constitutes a driven system with a rich nonlinear flow regime. Experimentally recovered toroidal formations of this system have motivated study of its volumetrically driven–dissipative vortex flow dynamics using two-dimensional hydrodynamics in the incompressible Navier-Stokes regime. Nonlinear equilibrium solutions are obtained for this system where a nonuniformly driven two-dimensional dust flow exhibits distinct regions of localized accelerations and strong friction caused by stationary fluids at the confining boundaries resisting the dust flow. In agreement with observations in experiments, it is demonstrated that the nonlinear effects appear in the limit of small viscosity, where the primary vortices form scaling with the most dominant spatial scales of the domain topology and develop separated virtual boundaries along their periphery. This separation is triggered beyond a critical dust viscosity that signifies a structural bifurcation. Emergence of uniform vorticity core and secondary vortices with a newer level of identical dynamics highlights the applicability of the studied dynamics to gigantic vortex flows, such as the Jovian great red spot, to microscopic biophysical intracellular activity.

DOI: 10.1103/PhysRevE.95.033204

I. INTRODUCTION

The dissipative systems that are driven to an enduring nonequilibrium state by a continuing source of free energy are a paradigm for a wide range of living and nonliving systems [1–3]. Nonequilibrium systems of this kind form stimulated and stable patterns, and recover, as a result of interventions from surroundings, to show first a formal signature of being responsive (*alive*), in clear distinction from their nonliving or purely entropy maximizing counterparts, like most museum exhibits that simply follow the Clausius' principle [3]. These responsive systems show a vast dynamic memory by their capacity and range of response to a continuum of stimuli from their surroundings, each of which may invoke a unique response, like making them erupt into a unique pattern. In its simplest form, a behavioral transition to such a state occurs, for example, in a system of Brownian particles irreversibly diffusing through a medium [4] when they are additionally subjected to a drive by a streaming medium and restricted in space by a confining potential or boundary. This results in a variety of their particle distributions for respective combinations of potential, boundary, and flow topologies [5]. A more correlated fluidlike phase of charged microparticles, suspended in the plasma state of matter [6–10], shows an even larger range of patterned response already in the linear regime of its dynamics [11–14] as a more realistic and rich nonlinear regime of it remains yet unexplored [3].

While microscopic characteristics of dusty plasmas are well known to resemble the crystalline [15–17] to viscoelastic fluidlike [18,19] media, the macroscopic dynamics of its fluidlike phase represents vortex activity in many volumetrically driven complex and biophysical fluids at very accessible scales. This dynamical range potentially covers low-Reynolds-number life-supporting dynamics of intracellular fluid or microcirculation of blood in lymphatic capillaries ($\mathrm{Re} < 1$), to high-Reynolds-number enormous scale circulations like the Jovian great red spot ($\mathrm{Re} > 10^2$). The first application of a two-dimensional (2D) hydrodynamic model to these volumetrically driven dust vortices was done to systematically formulate the vortex dynamics of dusty plasmas observed in normal laboratory conditions, as well as in microgravity conditions, on board the International Space Station (ISS) [20]. The results of these linear studies, successfully predicting multiplicity of vortex [13,14] and outlining basic scaling of boundary effects at low to moderate Reynolds numbers [11], still leave out the nontrivial physics of the often-noted transition to nonlinear regime of these vortices. Recently observed compelling nonlinear features of dust-vortex dynamics [12] promise to shed light on several less understood aspects of natural flows. For example, a nearly uniform vorticity in the core of a toroidal dust cloud observed in a higher flow velocity limit resembled high-Reynolds-number flow phenomena of the Jovian great red spot [21,22]. More noticeably, nonlinear phenomena, displayed also by dust dynamics, are proving to be a natural timing mechanism for biological systems, with growing evidence that processes like cell division are timed by critical transitions on approaching a threshold size rather than a preprogrammed linear evolution [23]. For example, the low-Reynolds-number intracellular mitotic activity taking place in cytoplasmic medium examined in budding yeast shows that the cells born smaller than normal size spend longer duration in the initial G1 phase until they reach a critical size for division, reproducing normal size offspring [24]. Nonlinear critical transitions thus provide a potential mechanism that monitors cell size and uses this information to regulate progression through events of the cell cycle, determining cell size and age, namely, the fundamental limiting factors for overall evolution of carbon-based life [23,25].

Equating the influence of chemical inhibitors of protein synthesis and polymerization by that of the inertial flow in a dusty plasma vortex, both of which must undergo criticality for continued stabilization by diffusion-dominated viscous transport at optimum scale, one gets a very primitive model for size regulation of a biophysical cell via a nonlinear threshold [26]. The equilibrium dusty vortex dimensions in a nonlinear operating regime are similarly asserted by the dynamics at a critical separation threshold rather than governed

*modhugamba@gmail.com

by the boundary geometry. This meaningful isomorphism is, however, quantifiable only by a systematic nonlinear formulation of the dusty plasma vortex dynamics. The present paper approaches this objective by discussing in Sec. II the essential two-dimensional toroidally symmetric, axially and radially bounded setup considered in the present formulation. Relevant to both the recent dusty plasma experiments and majority of microscopic flow arrangements in nature, this setup is considered with a radially sheared and axially uniform ion flow driving the constrained dust dynamics. The methodology of nonlinear solutions is presented in Sec. III, followed by the characterization of solutions in Sec. IV. The signature of nonlinearity in the form of uniform vorticity in the vortex core is discussed in Sec. IV, where this uniformity is additionally shown confirming with gigantic scale circulations like the great Jovian red spot. In Sec. IV C the phenomena of the boundary layer separation is investigated as a structural bifurcation of the 2D nondivergent vector fields with kinematic dust viscosity μ acquiring the role of a bifurcation parameter. Section IV D provides a nonlinear scaling, allowing one to estimate μ using velocimetric parameters of dust-vortex flow. Summary and conclusions are presented in Sec. V.

II. 2D NONLINEAR HYDRODYNAMIC MODEL

Similar to earlier linear approaches [11,14], the geometry of confined dust fluid is considered identical to the recent experiments where a toroidal dust structure forms having a poloidal dust flow in a glow discharge plasma [12,13], shown in Fig. 1. The dust fluid in this setup is suspended in the plasma and is spatially confined. The confinement or localization of the dust fluid in these and similar laboratory experiments is achieved effectively by a combination of electrostatic and gravitational fields where a two- or three-dimensional (3D) conservative field $\mathbf{F_c} = -\nabla V$ is achievable by various experimental means [17,27–30]. The potential well confining the dust must have closed contours that are allowed to have arbitrary shapes determined by effective dust confining potential. Considering a nearly incompressible dust fluid in a dynamical equilibrium, as described in Fig. 2, the interior of a highest potential contour confining the dust fluid is filled up uniformly by the fluid and without leaving any void or density variation. In an azimuthally symmetric, toroidally confined dust fluid recovered in the experiments, the dust fills a volume of the torus which is allowed to have an arbitrary shaped cross section determined by the confining potential. For analytic simplicity this cross section of the torus is approximated in the present treatment as a rectangle, as illustrated schematically in Fig. 2. Accordingly, using cylindrical coordinates to accommodate the azimuthal symmetry, the toroidal dust fluid is considered confined by an effective potential $V(r,z)$ within the boundaries of a finite section of an infinite cylinder of flowing plasma, or in the region where $0 < r/L_r < 1$ and $-1 < z/L_z < 1$, with no variation along the azimuthal dimension $0 < \phi < 2\pi$. It is assumed that the confining potential jumps from a constant value V_0 to a very high value at the rectangular boundary, providing a rectangular contour for perfect confinement.

For the dust flow that follows the incompressibility condition and has a finite viscosity, the dynamics is governed by the Navier-Stokes equation in which the drive produced by the ion

FIG. 1. Toroidal dust cloud with poloidal circulation in the laboratory dusty plasma experiment.

drag and the friction produced by the stationary neutral fluid can be suitably accounted for [31],

$$\frac{\partial \mathbf{u}}{\partial t} + (\mathbf{u}\cdot\nabla)\mathbf{u} = -\frac{\nabla P}{\rho} - \nabla V + \mu\nabla^2\mathbf{u} - \xi(\mathbf{u}-\mathbf{v}) - \nu(\mathbf{u}-\mathbf{w}). \quad (1)$$

Here $\mathbf{u}$, $\mathbf{v}$, and $\mathbf{w}$ are the flow velocities of the dust, ion, and neutral fluids, respectively. P and ρ are the pressure and mass density of the dust fluid, respectively, $V(r,z)$ is the confining potential, μ is kinematic viscosity, ξ is coefficient of ionic drag acting on the dust, and ν is the coefficient of friction generated by the stationary neutral fluid [32–34]. The overall combination of charged dust and background plasma is quasineutral and the electrons are in thermal equilibrium with the streaming ions and the confined dust. The incompressibility of the confined dust component is ensured by the expression

$$\nabla\cdot\mathbf{u} = 0, \quad (2)$$

which allows defining a streamfunction ψ such that $\mathbf{u} = \nabla\times(\psi\hat{\phi})$, with corresponding velocity components,

$$u_r = -\partial\psi/\partial z \text{ and } u_z = \frac{1}{r}\frac{\partial(r\psi)}{\partial r}. \quad (3)$$

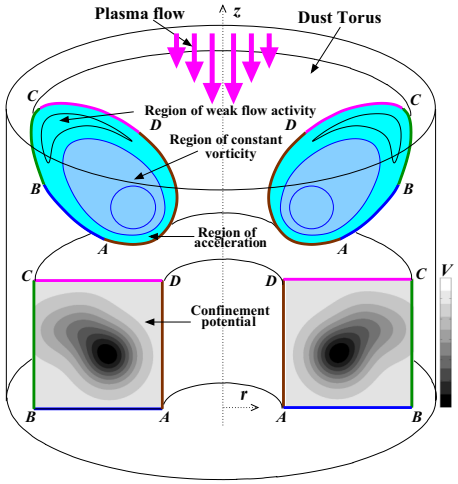

FIG. 2. Schematic representation of the toroidal dust cloud with vortex motion and mapping of the boundary of its cross section to a toroidal domain of rectangular cross section accommodated in the cylindrical geometry of the present nonlinear solutions. Segments AB, BC, CD, and DA of the cloud boundary map to the corresponding sides of the rectangle $ABCD$.

In case of an azimuthally symmetric dust flow, the dust motion can suitably be treated in the two-dimensional r-z plane such that the dust vorticity vector $\vec{\omega} = \nabla \times \mathbf{u}$ is directed purely along $\hat{\phi}$. Using these definitions in Eqs. (1) and (2) and stationary neutrals ($\mathbf{w} = 0$), we obtain, for a time-independent force equilibrium of dust flow field,

$$\nabla^2 \psi = -\omega, \tag{4}$$

$$(\mathbf{u} \cdot \nabla)\omega = \mu \nabla^2 \omega - (\xi + \nu)\omega + \xi \omega_s, \tag{5}$$

where ω_s is the vorticity of the ion fluid. The 2D solutions of (4) and (5) were recently obtained in the linear regime, or the low-Reynolds-number regime ($\mathrm{Re} = Lu/\mu \to 0$), where the inertial effects are dominated by the diffusive transport and nonlinear term in the left-hand side of the Eq. (5) could be neglected. The linear results allowed analysis of the almost laminar dust-vortex structures involving slow dust motion in the recent laboratory experiments where various single and multiple dust-vortex form driven by nonuniformity of the plasma flows and parameters. Interestingly, a detailed nonlinear regime of strong dust-vortex flow is routinely observable in these experiments where driven vortices with strong circulations are surrounded in the region of weak drive either by secondary vortices that are co- and countercirculating, or the stagnant regions of almost no circulation such that very sharp and localized flow velocity gradients are maintained inside the dust volume [12]. Usually termed as more complex dust flow patterns and excluded from the simpler interpretations, we show that these configurations are well represented by the nonlinear solutions of the system (4) and (5), as obtained in the following section.

III. NONLINEAR SOLUTION PROCEDURE

Equations (4) and (5) are solved in the present work by retaining the nonlinear term in the left-hand side of Eq. (5), which becomes comparable to the source and diffusion terms in the right-hand side in the limit of large flow velocity. Equation (5) in linear limit admits standard solution procedures where integration is possible for an individual mode of the dust vorticity interacting with that of the driver. As presented by the authors in Ref. [11], such first 2D linear solutions excluding the nonlinear term were obtained by constructing an eigenvalue problem and representing the dust and source streamfunctions in terms of a set of orthogonal eigenfunctions that satisfy the appropriate boundary conditions. The nonlinear solutions are, however, nontrivial, and even a numerical approach to them in two dimensions must involve an iterative procedure as adopted in the present study.

In the first step, the equations are cast in the form suitable for numerical solutions in order to yield numerical solutions with enough accuracy. This is achieved by ensuring that the two residues, R_1 and R_2, defined, respectively, as

$$\frac{\Delta\psi}{\Delta L^2} = \nabla^2 \psi + \omega, \tag{6}$$

$$\frac{\Delta\omega}{\Delta L^2} = \nabla^2 \omega - \frac{1}{\mu}(u \cdot \nabla)\omega - \frac{(\xi + \nu)}{\mu}\omega + \frac{\xi}{\mu}\omega_s, \tag{7}$$

are sufficiently smaller than the corresponding tolerance after successive iterations. Using cylindrical coordinates (r, ϕ, z) where all variations are in the r-z plane, Eqs. (6) and (7) reduce to

$$\psi^{n+1} = \psi^n + \Delta L^2 \left(\frac{\partial^2}{\partial r^2} + \frac{1}{r}\frac{\partial}{\partial r} - \frac{1}{r^2} + \frac{\partial^2}{\partial z^2} \right) \psi^n + \Delta L^2 \omega^n, \tag{8}$$

$$\omega^{n+1} = \omega^n + \Delta L^2 \left(\frac{\partial^2}{\partial r^2} + \frac{1}{r}\frac{\partial}{\partial r} - \frac{1}{r^2} + \frac{\partial^2}{\partial z^2} \right) \omega^n - \frac{\Delta L^2}{\mu} \left(u_r \frac{\partial \omega}{\partial r} \right)^n - \frac{\Delta L^2}{\mu} \left(u_z \frac{\partial \omega}{\partial z} \right)^n - \Delta L^2 K_1 \omega^n + \Delta L^2 K_2 \omega_s, \tag{9}$$

where $\Delta\psi \equiv \psi^{n+1} - \psi^n$, $K_1 = (\xi + \nu)/\mu$, and $K_2 = \xi/\mu$, and the integer n represents the index of the iteration. In our numerical solution procedure, the iterations are made by updating the ω and ψ fields until the minimum values of the residues R_1 and R_2 below a reasonably small tolerance are achieved.

IV. NONLINEAR DUST VORTEX FLOW SOLUTIONS

The converged solutions are obtained for the confined dust in the toroidal domain having a rectangular cross section where the driving plasma flow velocity v is directed along $-\hat{z}$ and has only a radial variation of the form of a Bessel function j_0 as presented in Fig. 3(a) with associated source vorticity ω_s plotted in Fig. 3(b). Driven by this plasma flow field in the domain of confinement, the dust streamfunction is determined iteratively by imposing the boundary conditions such that the dust velocity normal to the boundaries is zero. Consequently, the dust is well confined in a finite section of a cylinder that accommodates the torus having a rectangular cross section in the r-z plane. The boundary conditions are motivated by the high-shear experimental configurations where the driver is localized in a narrow region of the domain, and in the region of domain far from the influence of the driver the dust experiences strong friction such that velocities there are considerably small (see schematic Fig. 2 and Ref. [12]). Accordingly, the dust velocity follows no-slip boundary conditions for all the physical boundaries confining the dust. However, at the vertical boundary imposed by symmetry at the cylinder center ($r \to 0$), where the driving ion flow velocity is strongest, the magnitude of the dust velocity is not controlled by the boundary condition. A governing factor, all the derivatives at $r = 0$ vanish owing to the cylindrical symmetry of the domain and radial component

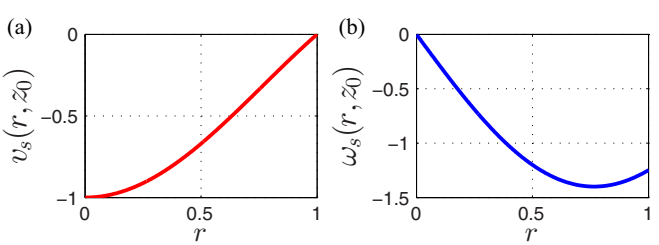

FIG. 3. Profiles of the (a) driver velocity v and (b) corresponding driver vorticity ω_s which are uniform along $\hat{z}$ and $\hat{\phi}$.

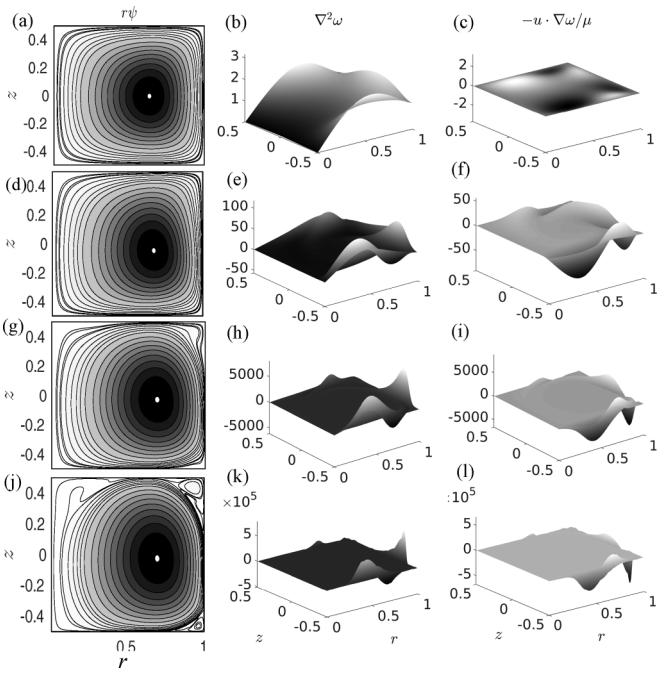

FIG. 4. (a) Dust flow streamlines, strengths of (b) the diffusive term and (c) the nonlinear term plotted from top to bottom for the values of dust viscosity $\mu = 1\times10^{-3}$, 1×10^{-4}, 1×10^{-5}, and $8\times10^{-7}U_0L$, respectively, where the values $\nu = 0.01\ U_0/L$ and $\xi = 0.001U_0/L$ are used.

of the dust velocity, vanishes at this boundary by natural symmetry of the cylindrical setup.

The complete nonlinear solutions describing the driven dust dynamics in terms of 2D flow streamlines and the corresponding ψ and ω fields are presented for small- to high-Reynolds-number regimes in Fig. 4. The length and velocities in the present analysis are scaled to the system length or the domain dimension $L \equiv L_r = L_z$ and vertically downward streaming ion velocity magnitude U_0, respectively. The parameters ξ, μ, and ν accordingly have units derived from these scales. The entire analysis is done using a common combination of driver velocity and corresponding vorticity profiles presented in Figs. 3(a) and 3(b), respectively. Considering a typical laboratory glow discharge argon plasma with micron-size dust with parameters $n \simeq 10^9$ cm^{-3}, $T_e \simeq 3$ eV, $T_i \simeq 1$ eV, largely at the sheath entrance where ions are streaming with a flow velocity U_0 equivalent to the fraction of the ion acoustic velocity, $c_s = \sqrt{T_e/m_i}$. The value of ion drag coefficient can be estimated as $\xi \approx 10^{-4}U_0/L$, and the neutral collision frequency can be $\nu \approx 10^{-2}U_0/L$ [32–34]. For a typical system size, $L \approx 10$ cm, the range of kinematic viscosity μ can similarly be chosen $\mu \approx 6\times10^{-4}U_0L$, which corresponds to small Reynolds numbers ($Rn \simeq 1$) of the dust flow consistent with the linear viscous regime.

The dust flow streamlines, which in cylindrical setup are the equal height contours of the product $r\psi$ in the r-z plane, are plotted in the first column of frames in Fig. 4 for the parameters $\xi = 0.001U_0/L$ and $\nu = 0.01U_0/L$. The effect of change in the dust kinematic viscosity, from a higher value $\mu = 1\times10^{-3}U_0L$ to a lower value $\mu = 8\times10^{-7}U_0L$, is visible

TABLE I. Parameters μ and resulting values of Δr_b, u_b, and Re in the analysis.

$\mu\ [U_0L]$	$u_b\ [U_0]$	$\Delta r_b\ [L]$	Re
1×10^{-3}	0.0024	0.1387	0.336
1×10^{-4}	0.0116	0.1030	11.961
1×10^{-5}	0.0217	0.0456	99.141
1×10^{-6}	0.0254	0.0198	503.705
8×10^{-7}	0.0252	0.0178	561.600

on examining the results plotted from the top to bottom row of frames in Fig. 4 where μ reduces, taking the values 1×10^{-3}, 1×10^{-4}, 1×10^{-5}, and $8\times10^{-7}U_0L$, respectively. Also shown in the second and third columns of Fig. 4 are the strengths of the most dominant term $\nabla^2\omega$ and the nonlinear term $-\mathbf{u}\cdot\nabla\omega/\mu$, respectively, showing the increasing strength of the nonlinearity, which is increasingly balanced by the viscous diffusion at decreasing μ values. For example, as clearly visible from Fig. 4, the diffusive term is much larger and entirely uncorrelated to nonlinear terms for large μ values, or in the frames (b) and (c). For the small μ value cases presented in frames (k) and (l), the most interesting variation is present in the boundary regions of the solution of Eq. (5), which is produced entirely by the balance $\nabla^2\omega - \mathbf{u}\cdot\nabla\omega/\mu \approx 0$, as the contribution of other terms remains nearly negligible. As we analyze in the following sections, the boundary in this regime provides the strongest source of vorticity at smaller scales, which can be dissipated in the domain volume at a relatively slower rate than the linear case after being convected away in the interior along the streamlines.

For the system (4) and (5) with applied boundaries, the values of width Δr_b of the boundary region, bulk flow velocity u_b, and Re are provided in Table I in the range of transition corresponding to the range of μ values used in the present analysis. Note that the saturation of the width Δr_b is in departure from the linear boundary layer scaling $\Delta r_b \propto \mu^{1/3}$ [11] and relates to nonlocal diffusion of vorticity convected along streamlines. This convection governs a number of nonlinear aspects of the dust-vortex flow addressable under the present formulations. The dominant nonlinear features of high-Re solutions described below include (i) a persistent uniform vorticity core of the vortex, (ii) development of a separated convective boundary layer via a critical phenomenon analogous to certain biophysical processes, and (iii) a nonlinear boundary layer scaling prescribing velocimetric determination of the dust viscosity.

A. Persistent uniform vorticity solutions at high Reynolds number

The strength of the nonlinear term $\mathbf{u}\cdot\nabla\omega$ in Eq. (10) can be examined for our solutions based on the properties of dependence $\omega(\psi)$ in a 2D setup. For ω purely a function of ψ the term must vanish, as can be shown by substituting the definitions $\mathbf{u} = \nabla\times\psi\hat{\phi}$ and a formal solution $\omega = f(\psi)$ of $\nabla^2\psi = -\omega$ in $\mathbf{u}\cdot\nabla\omega$:

$$\mathbf{u}\cdot\nabla\omega = (\hat{\phi}\times\nabla\psi)\cdot\nabla(f(\psi)). \tag{10}$$

Note that the right-hand side represents a dot product of two orthogonal vectors which must vanish for all ψ, implying that

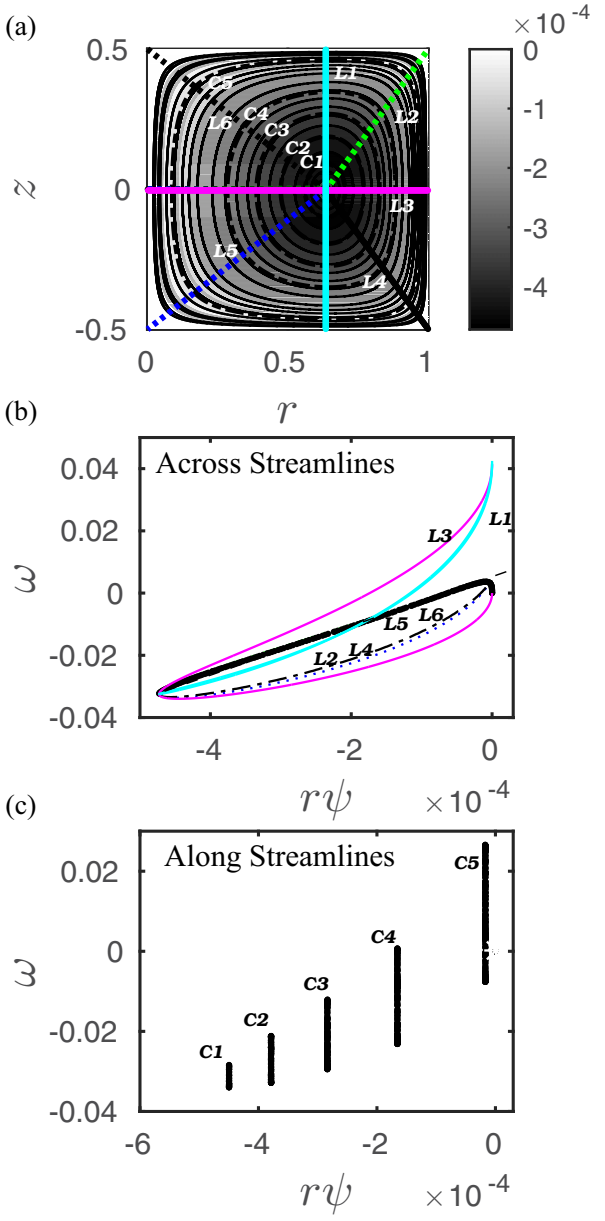

FIG. 5. (a) Dust flow streamlines superimposed by straight lines and contours used to draw profiles of ω as function of $r\psi$, (b) vorticity ω as function of $r\psi$ along the straight line segments ($L1, L2, L3, L4$, and $L5$) joining the vortex center to the domain vortices, and (c) that along the indicated contours ($C1, C2, C3, C4$, and $C5$). The profiles correspond to $\mu = 10^{-3}\, U_0 L$, $\xi = 0.001\, U_0/L$, and $\nu = 0.01\, U_0/L$.

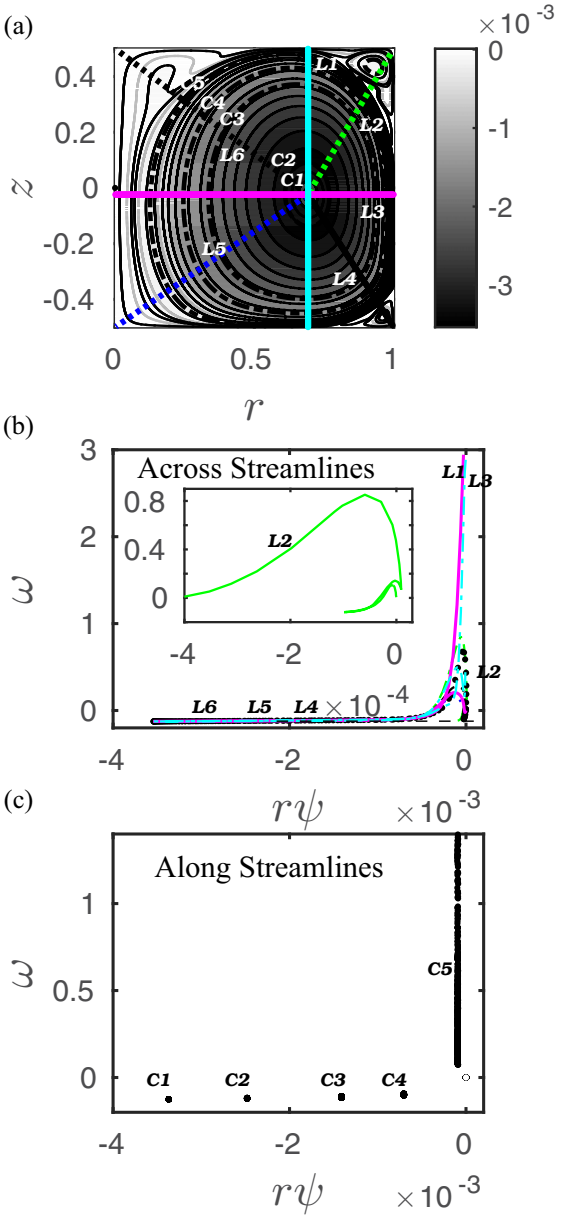

FIG. 6. (a) Dust flow streamlines superimposed by straight lines and contours used to draw profiles of ω as a function of $r\psi$, (b) vorticity ω as function of $r\psi$ along the straight line segments ($L1, L2, L3, L4$, and $L5$) joining the vortex center to the domain vortices, and (c) that along the indicated contours ($C1, C2, C3, C4$, and $C5$). The profiles correspond to $\mu = 8\times10^{-7}$ $U_0 L$, $\xi = 0.001\, U_0/L$, and $\nu = 0.01\, U_0/L$.

the nonlinear term $\mathbf{u}\cdot\nabla\omega$ must vanish where ω is either a pure function ψ or uniform. For application to the present cylindrical setup where the contour parameter is $r\psi$ rather than ψ, this result readily transforms in the condition that the nonlinear convection vanishes when ω is purely a function of $r\psi$. For our solutions it is noted that at high μ, although the nonlinear term has a small magnitude it remains finite, since ω shows a dependence on the product $r\psi$ as well as on r and z. For the low-μ (high Re) solutions, however, the vorticity ω remains almost independent of r and z in the interior and is purely a function of $r\psi$, except in (and beyond) a thin boundary layer region.

This dependence is characterized in Figs. 5 and 6 for high- and low-μ cases, respectively. The contours of $r\psi$ are plotted in subplot (a) of Figs. 5 and 6. The dependence $\omega(r\psi)$ is examined by plotting the variation of ω in space both when $r\psi$ is allowed to change [across streamlines, by following the solid lines, in subplot (b)] and when $r\psi$ is kept constant [along streamlines, by following the dashed contours, in subplot (c)]. The strong variation in the boundary region of the high-μ case

(Fig. 6) shows that the function of the nonlinear term is to prevent the diffusion of externally produced large vorticity to the interior region by convecting it away along the streamlines in the boundary layer. The constant net vorticity of the core region is hence conserved. This nonlinear balance allows the setup of a nearly rigid bodylike motion of the vortex core with $v \propto r$ and a constant vorticity both in laboratory experiments and in natural flows.

We are now in a position to compare both low- and high-μ limits accessible in laboratory experiments with a vortex formation in nature at phenomenally different scales than those of ordinary dusty plasma experiments. A highly persistent vortex structure like the Jovian great red spot (GRS), Jupiter's largest anticyclonic vortex, measuring approximately 22 000 × 11 000 km, for example, displays zonal eastward velocity velocity profiles [21] in close agreement with the large-Re (small μ) case plotted in Fig. 6, where a uniform vorticity core is surrounded by zones of sharp vorticity gradients. The similar velocity profiles are observed in relatively younger, year 1939 originated, pair of anticyclonic Jovian white ovals that are separated by teardrop-shaped cyclonic vortex. In the interior region of closed streamlines the additional uniformity of ω with respect to the product $r\psi$ in the low-μ case (Fig. 6) is in confirmation of a toroidal analog of the integral condition obtained by Batchelor [35],

$$\frac{\partial \omega}{\partial(r\psi)} \oint r(u_r \hat{r} + u_z \hat{z}) \cdot d\mathbf{l} = 0,$$

which applies to the streamlines in the interior region as the integral evaluated along these closed streamlines vanishes for these solutions, requiring ω to be independent of the product $r\psi$ in the core.

B. Boundary layer separation and secondary vortex formation

For our high-μ case solutions, the boundary layer forms all along the domain boundary where a no-slip condition is applied and ψ remains monotonic in the direction orthogonal to streamlines. In low-μ cases, however, the flow in the regions of sharp corners features an arrangement of smaller co- and counter-rotating vortices and ψ shows oscillatory spatial variation orthogonal to streamlines with a variety of scales, as highlighted in the subplot drawn in Fig. 6(b). When driven at the same scale, the scale length of the largest vortex in this regime is still determined by the dimension L of the domain, while the surrounding secondary corotating vortex has a smaller spatial scale length of $\sim(\sqrt{2}-1)L$. This factor corresponds to the corner zones of a square domain which accommodates a primary vortex of diameter $\sim L$. The region between two corotating vortices is further populated by somewhat elongated and weak counter-rotating teardroplike vortices as shown in Fig. 6(a). The strength of the secondary small-scale vortex structures is, however, subject to the magnitude of the dust viscosity. At higher dust viscosity the large momentum diffusivity begins to prevent the formation of small-scale structures, as presented in Figs. 5(a) and 5(b), where the dust flow streamlines and ω values are plotted, respectively, using $\mu = 10^{-3} U_0 L$.

For a low-μ case, Figs. 7(a) and 7(b) present strengths of diffusive and nonlinear source terms for vorticity, respectively,

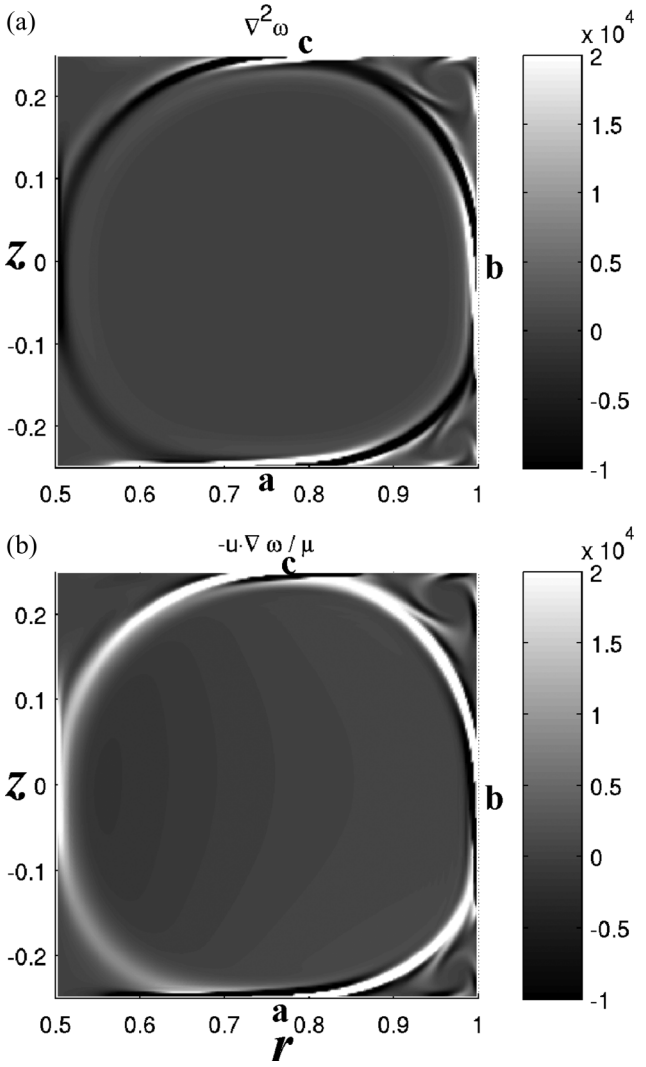

FIG. 7. (a) Magnitude of the diffusion term and (b) magnitude of the nonlinear term plotted for $\mu = 8\times10^{-7}\ U_0 L$, $\xi = 0.001\ U_0/L$, and $\nu = 0.01\ U_0/L$ in a domain confinement limited to larger r values.

in a set of solutions obtained for a confinement domain limited to larger r values ($0.5 < r < 0.1$) for clarity. The interface of the central vortex with the domain boundary is strongly localized at a few points (indicated as **a**, **b**, and **c**) of closest approach from the center, ($\sim L/2$), while elsewhere it is only via a nearly circular shear layer running along the rest of the boundary of the strongest vortex. The vorticity generated by interaction of the central vortex with the no-slip domain boundary is being convected away from points **a, b**, and **c** along the streamlines in Fig. 7(b), as the convective nonlinear term has large positive value along these streamlines. This convected vorticity is, in turn, diffused away steadily across the streamlines, owing to the sharp velocity gradient, by the diffusion term which displays an identical variation but with negative magnitude. Although the velocity gradients and diffusion are higher along the shear layer, they are relatively much more moderate as compared to the those required in the linear model where the convection channel is unavailable and a sharp boundary layer must exist in order to diffuse the

vorticity generated at the no-slip boundary purely across the streamlines.

C. Separation as structural bifurcation at critical viscosity

We now address the nonuniformity of the flow structure along the domain boundary at high μ. Although the ideas related to Prandtl-Batchelor boundary flows and their breakdown in various limits have long existed and are thoroughly reviewed [36], it is only somewhat recently that development of such nonuniformity and transition to a separated boundary layer was shown to be a structural bifurcation of the 2D flow characteristics [37,38]. For time-dependent or turbulent flows this bifurcation was identified to take place at a critical value of time $t = T^*$ that corresponds to the breakdown of a monotone vorticity profile in the boundary layer. We note that in our steady-state flow formulation the kinematic viscosity μ assumes the role of bifurcation parameter, and this transition in our solutions takes place at a critical μ value. This criticality allows the bounded dust-vortex setup to represent a class of systems that can self-stabilize by making a critical transition to a self-similar state [26].

As discussed in [37], the solutions of the set formed by the Navier-Stokes and the incompressibility condition,

$$\frac{\partial \mathbf{u}}{\partial t} + (\mathbf{u}\cdot\nabla)\mathbf{u} = -\nabla\frac{P}{\rho} + \mu\nabla^2\mathbf{u}, \tag{11}$$

$$\text{and} \quad \nabla\cdot\mathbf{u} = 0, \tag{12}$$

with a no-slip boundary ∂M of a compact manifold M can be viewed as one-parameter families of divergence-free vector fields with parameter t. For such a family of divergence-free vector fields $\mathbf{u}(t)$, a structural bifurcation, or a change in topological equivalence class, occurs at a point in the spatial and parameter space if the normal derivative of the velocity field $\mathbf{u}_n = \partial\mathbf{u}/\partial\mathbf{n}$ has a degenerate singular point on the boundary segment ∂M such that for $\mathbf{u}_n$ there is a finite function of the parameter t, or $\partial\mathbf{u}_n/\partial t \neq 0$. Since the point of separation is also a spatially local extremum for the vorticity, it was concluded by applying the Hopf lemma that the vorticity gradient is directed outward or inward at this point. The presence of an adverse pressure gradient required for the separation in such divergence-free field systems follows directly from the fact that the tangential derivative of the pressure is exactly the normal derivative of the vorticity. Based on this relationship, the above bifurcation condition was shown in [37] to translate in terms of vorticity at the boundary ∂M, which essentially required that the vorticity profile must reach its first zero value along ∂M at a local minimum point while evolving with respect to the bifurcation parameter.

In Fig. 8, where ω is plotted for range of μ examined in our analysis, we show that this condition holds for our solutions at the frictional boundaries $\partial M \equiv AB$, BC, and CD (indicated by arrows at two of the boundaries visible in the figure), where such boundary layer separation takes place following interaction with the boundary of the primary vortex at points **a**, **b**, and **c** in our solutions (as marked in Fig. 7). For clarity, in Fig. 9 we present the profiles of vorticity along the boundary segment BC for various values of μ where the first zero value of vorticity coincides with the local minima of vorticity

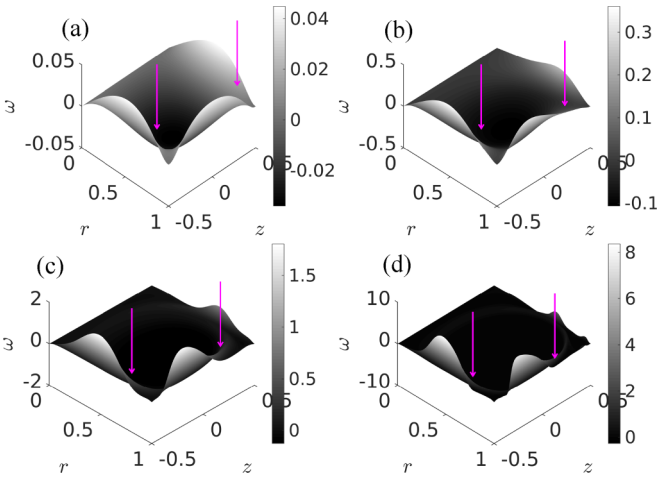

FIG. 8. The vorticity surface plots for values of parameter (a) $\mu = 10^{-3}$, (b) 10^{-4}, (c) 10^{-5}, and (d) $8\times10^{-7}U_0L$. The developing points of separation are indicated by arrows on segments AB and BC.

at a critical value $\mu^* \approx 1\times10^{-5}U_0L$ for our analysis. This location, $z \approx 0.29$, at the boundary BC is indicated by an arrow in Fig. 9. At this value $\mu = \mu^*$ the profile has a degenerate singular point that bifurcates, at lower μ values, into a set of two isolated points since the profile begins to intersect the axis $\omega = 0$ at two points above its minimum. Similarly, the values for μ^* for the separation at the boundaries AB and CD were noted to be $\approx3\times10^{-5}U_0L$ and $\approx2\times10^{-6}U_0L$, respectively, meaning that the separation is triggered at the highest μ value at the boundary AB, followed by the boundaries BC and CD. These values demarcate the range beyond which a nonlinear prescription needs to be applied for the local estimates. This critical behavior, accompanied by emergence of self-similar secondary structures, highlights the capacity of confined dusty plasma vortex structures to represent the complexity of biophysical processes where replication must follow a bifurcation [23]. The transition in our square-shaped setup produces an identical structure only with a scale ratio of $\sim1 : (\sqrt{2}-1)$. Interestingly, a recent experiment [39] with dust vortices has indeed shown a transition resulting in secondary dust vortices with scale ratio of unity, which is isomorphic to the process of cell mitosis triggered by a bifurcation and is being addressed by a distinct parameter regime of our formulation.

D. Velocimetric prescription of the dust viscosity

We finally note that beyond the boundary layer separation (BLS) transition at μ^*, a very simple relationship exists between the velocimetrically obtainable quantities and dust viscosity. This should allow one to estimate the dust viscosity using velocimetry techniques, for example, computer-aided particle imaging velocimetry (PIV), which provides local velocity and vorticity in the vortex [12,40,41]. Since we observe from the characterization of nonlinear solution that the vorticity diffusion across the streamlines is nearly balanced by the nonlinear convection of the vorticity, the balance (5) in the convection-dominated boundary layer reads

$$\mu\nabla^2\omega = \mathbf{u}\cdot\nabla\omega. \tag{13}$$

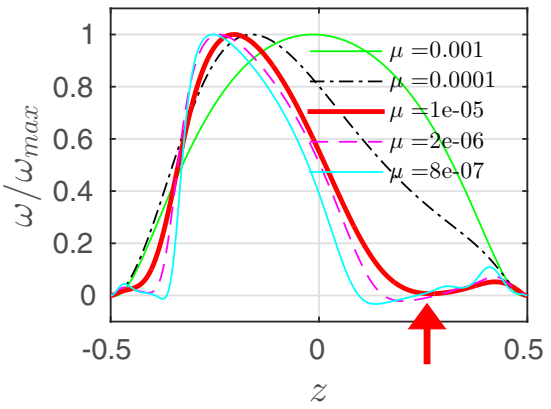

FIG. 9. The normalized vorticity profile along the no-slip boundary BC for various values of parameter μ. The point of separation and associated bifurcation is indicated by an arrow where the profile corresponding to the critical value $\mu^* \approx 10^{-5} U_0 L$ has a single degenerate singular point.

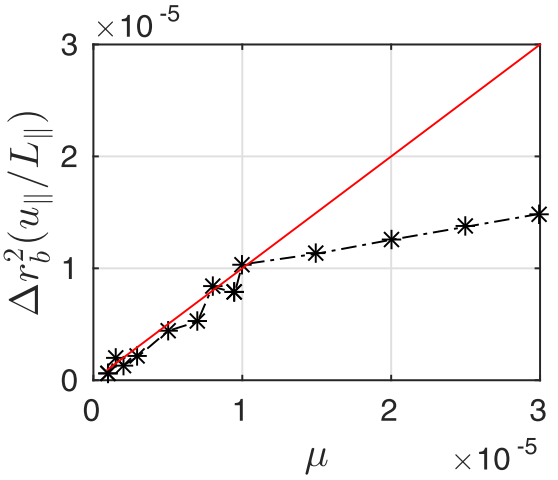

FIG. 10. The nonlinear boundary layer scaling with dust viscosity μ. The profile shows a change of regime at $\mu^* \approx 1 \times 10^{-5} U_0 L$.

Note that the right-hand side involves the convective derivative of the vorticity ω parallel to streamlines, while the left-hand side has a diffusion purely orthogonal to the streamlines. At any given point in the boundary layer the balance (13) therefore has a simple form,

$$\mu \frac{\omega}{\Delta r_b^2} = u \frac{\omega}{L_\parallel}, \tag{14}$$

where Δr_b is the velocity gradient scale length, or approximately the boundary layer width, and $L_\parallel = u/u'$ is the gradient scale length of the velocity along the streamlines (with the prime indicating a derivative along the streamlines). This readily provides the nonlinear version of the boundary layer width scaling with the viscosity μ as

$$\mu = \Delta r_b^2 \frac{u}{L_\parallel}, \tag{15}$$

indicating that in the BLS regime, the dust viscosity may be evaluated from the experimentally determinable quantities, namely, boundary layer width, dust velocity, and its gradient length along the streamlines. In Fig. 10 we have plotted the quantity $\Delta r_b^2 u/L_\parallel$ as a function of viscosity μ, showing that beyond the BLS transition ($\mu < \mu^* \approx 1 \times 10^{-5} U_0 L$ on segment BC) this quantity is equal to the viscosity μ. However, a clear disagreement is triggered below the critical BLS transition and at larger μ the linear scaling [11] can be recovered.

V. SUMMARY AND CONCLUSIONS

The nonlinear properties of a volumetrically driven 2D dust-vortex flow of a confined dust fluid suspended in a plasma are studied. Motivated by toroidally symmetric flow formation and signatures of the nonlinear nature of its flow dynamics at higher dust velocities, 2D nonlinear equilibrium solutions of the vortex flow are obtained in a toroidally symmetric domain. The solutions obtained in the present treatment are relevant to a large number of observations in dusty plasmas setups where a vigorous dust-vortex flow dynamics is observed with flow velocities approaching the nonlinear limit. The solutions are in confirmation with experiments where a localized dust vortex is seen surrounded by regions with a relatively moderate or negligible dynamical activity.

Similar to observations of a dust torus where poloidal dust flow is recoverable with considerably uniform vorticity, the driven primary vortex in the present solutions is formed with almost uniform vorticity in the core, surrounded by region a strong variation of vorticity value and oscillatory nature of streamfunction. The relationship between vorticity ω and product $r\psi$ is examined in the small- and large-Reynolds-number regimes to recover independence of ω from $r\psi$ in the uniform vorticity core formed at large Reynolds number. In this limit the core vorticity follows the curvilinear form of an integral condition on the regions of closed streamlines where boundary conditions are no longer usable for determination of ω in the high-Reynolds-number regime and its analytic value remains largely indeterminate.

In the presence of 2D heterogeneous boundary conditions applied to dust flow in a curvilinear coordinate system, the major nonlinear effects cause the boundary layer to separate from the domain boundary. This causes the vorticity generated from the interaction with the no-slip, or frictional, boundaries to be convected away with strong flows of the primary vortices. The separation allows dynamic isolation of the regions scaling with the dimensions of small-scale features of the boundary (e.g., spatial modulations or the sharp corners) and development of secondary vortices in these regions. The development of a separated boundary layer is investigated as a structural bifurcation where the kinematic viscosity assumes the role of the bifurcation parameter and the separation coincides with the bifurcation. The bifurcation is shown to occur when the vorticity profile approaches its first zero value along the boundary at the point where its minimum is located. This critical behavior and signatures of equivalent nonlinear vortex states in experiments indicates the capacity of confined dusty plasma vortex structures to represent a class of systems that can self-stabilize by making a critical transition to a self-similar state, for example, biophysical transition during cells undergoing mitosis. The nonlinear scaling of the boundary layer parameters with kinematic viscosity μ is obtained and a critical value μ^* demarcating the transition

to a nonlinear regime is identified. These two factors allow estimation of the viscosity of charged fluids using appropriate scaling by identifying a structural change in the flow patterns in experiments. The nonlinear dust-vortex dynamics thus offers quantitative insight and an analytic framework to a number of natural systems that dusty plasmas emulate.

[1] I. Prigogine and R. Balescu, Acad. Roy. Belg. Bull. Clin. Sci. **41**, 917 (1955).
[2] P. Glansdorff and I. Prigogine, Physica **20**, 773 (1954).
[3] J.-M. Andr, Rev. Quest. Sci. **177**(3-4), 323 (2006).
[4] A. Einstein, Ann. Phys. (Berlin, Ger.) **322**, 549 (1905).
[5] L. Holzer, J. Bammert, R. Rzehak, and W. Zimmermann, Phys. Rev. E **81**, 041124 (2010).
[6] G. E. Morfill, H. M. Thomas, U. Konopka, H. Rothermel, M. Zuzic, A. Ivlev, and J. Goree, Phys. Rev. Lett. **83**, 1598 (1999).
[7] V. E. Fortov, O. S. Vaulina, O. F. Petrov, V. I. Molotkov, A. V. Chernyshev, A. M. Lipaev, G. Morfill, and H. Thomas, J. Exp. Theor. Phys. **96**, 704 (2003).
[8] A. P. Nefedov, G. E. Morfill, V. E. Fortov, H. M. Thomas, H. Rothermel, T. Hagl, A. V. Ivlev, and M. Zuzic, New J. Phys. **5**, 33 (2003).
[9] G. E. Morfill, M. Rubin-Zuzic, H. Rothermel, A. V. Ivlev, B. A. Klumov, H. M. Thomas, U. Konopka, and V. Steinberg, Phys. Rev. Lett. **92**, 175004 (2004).
[10] M. Rubin-Zuzic, H. Thomas, S. Zhdanov, and G. E. Morfill, New J. Phys. **9**, 39 (2007).
[11] M. Laishram, D. Sharma, and P. K. Kaw, Phys. Rev. E **91**, 063110 (2015).
[12] M. Kaur, S. Bose, P. Chattopadhyay, D. Sharma, J. Ghosh, Y. Saxena, and E. Thomas, Jr., Phys. Plasmas **22**, 093702 (2015).
[13] M. Kaur, S. Bose, P. Chattopadhyay, D. Sharma, J. Ghosh, and Y. Saxena, Phys. Plasmas **22**, 033703 (2015).
[14] M. Laishram, D. Sharma, and P. K. Kaw, Phys. Plasmas **21**, 073703 (2014).
[15] H. Thomas, G. E. Morfill, V. Demmel, J. Goree, B. Feuerbacher, and D. Mohlmann, Phys. Rev. Lett. **73**, 652 (1994).
[16] H. Ikezi, Phys. Fluids **29**, 1764 (1986).
[17] O. Arp, D. Block, M. Klindworth, and A. Piel, Phys. Plasmas **12**, 122102 (2005).
[18] L. Pan, A. Morozov, C. Wagner, and P. E. Arratia, Phys. Rev. Lett. **110**, 174502 (2013).
[19] P. K. Kaw and A. Sen, in *Strongly Coupled Coulomb Systems*, edited by G. J. Kalman, J. M. Rommel, and K. B. Blagoev (Plenum, New York, 1998).
[20] H. M. Thomas, G. E. Morfill, V. E. Fortov, A. V. Ivlev, V. I. Molotkov, A. M. Lipaev, T. Hagl, H. Rothermel, S. A. Khrapak, R. K. Suetterlin *et al.*, New J. Phys. **10**, 033036 (2008).
[21] A. R. Vasavada, A. P. Ingersoll, D. Banfield, M. Bell, and P. J. Gierasch, Icarus **135**, 265 (1998).
[22] P. S. Marcus, Nature (London) **331**, 693 (1988).
[23] W. F. Marshall, K. D. Young, M. Swaffer, E. Wood, P. Nurse, A. Kimura, J. Frankel, J. Wallingford, V. Walbot, X. Qu *et al.*, BMC Biol. **10**, 101 (2012).
[24] J. J. Turner, J. C. Ewald, and J. M. Skotheim, Curr. Biol. **22**, R350 (2012).
[25] N. Meyer-Vernet and J.-P. Rospars, Phys. Biol. **13**, 066006 (2016).
[26] B. Pfeuty and K. Kaneko, Phys. Biol. **4**, 194 (2007).
[27] M. Klindworth, A. Melzer, A. Piel, and V. A. Schweiger, Phys. Rev. B **61**, 8404 (2000).
[28] S. Mitic, B. A. Klumov, U. Konopka, M. H. Thoma, and G. E. Morfill, Phys. Rev. Lett. **101**, 125002 (2008).
[29] M. A. Fink, S. K. Zhdanov, M. H. Thoma, H. Hofner, and G. E. Morfill, Phys. Rev. E **86**, 065401 (2012).
[30] M. A. Fink, S. K. Zhdanov, M. Schwabe, M. H. Thoma, H. Hofner, H. M. Thomas, and G. E. Morfill, Europhys. Lett. **102**, 45001 (2013).
[31] L. D. Landau and E. M. Lifshits, *Fluid Mechanics* (Pergamon Press, Oxford, England, 1987).
[32] M. S. Barnes, J. H. Keller, J. C. Forster, J. A. ONeill, and D. K. Coultas, Phys. Rev. Lett. **68**, 313 (1992).
[33] S. A. Khrapak, A. V. Ivlev, G. E. Morfill, and H. M. Thomas, Phys. Rev. E **66**, 046414 (2002).
[34] A. V. Ivlev, S. A. Khrapak, S. K. Zhdanov, G. E. Morfill, and G. Joyce, Phys. Rev. Lett. **92**, 205007 (2004).
[35] G. K. Batchelor, J. Fluid Mech. **1**, 177 (1956).
[36] O. A. Oleinik and V. N. Samokhin, *Mathematical Models in Boundary Layer Theory* (Chapman and Hall, London, 1999).
[37] M. Ghil, J.-G. Liu, C. Wang, and S. Wang, Physica D **197**, 149 (2004).
[38] M. Ghil, T. Ma, and S. Wang, Indiana Univ. Math. J. **50**, 159 (2001).
[39] M. Choudhary, S. Mukherjee, and P. Bandyopadhyay, arXiv:1701.03233.
[40] E. Thomas, Phys. Plasmas **6**, 2672 (1999).
[41] E. Thomas, Phys. Plasmas **13**, 042107 (2006).